Equilibrium critical thickness for misfit dislocations in III-nitrides

David Holec,[a] Yucheng Zhang, D. V. Sridhara Rao, Menno J. Kappers, Clifford McAleese, and Colin J. Humphreys
Department of Materials Science and Metallurgy, University of Cambridge, Pembroke Street, Cambridge CB2 3QZ, United Kingdom

(Received 24 July 2008; accepted 16 October 2008; published online 17 December 2008)

The critical thickness gives the transition point between fully strained and relaxed heteroepitaxial films and determines the onset of defect generation, including misfit dislocations, cracks, and V-pits. An important variable in critical thickness calculations concerning misfit dislocations is the dislocation energy. It consists of two contributions: the elastic energy of the bulk material around a dislocation and the energy of the dislocation core. The latter part is often neglected. Recent atomistic calculations have estimated this quantity together with the radius of dislocation cores in wurtzite III-nitrides. The effect of the dislocation core energy on equilibrium critical thickness values for III-nitrides is investigated theoretically and is shown to be significant. The calculated values of the critical thickness are compared with experimentally determined values of the critical thickness for misfit dislocations in the InGaN/GaN system using transmission electron microscopy and x-ray diffraction techniques. A comparison of the present model with experimental observations, together with a wide range of data from the literature for both AlGaN/GaN and InGaN/GaN systems, shows reasonable agreement. Finally, we speculate on a possible reason for differences between theory and experiment. © *2008 American Institute of Physics*. [DOI: 10.1063/1.3033553]

I. INTRODUCTION

Wurtzite gallium nitride (GaN) and its alloys are widely used in optoelectronic devices. Light emitting diodes incorporating InGaN/GaN and GaN/AlGaN epitaxial multilayers produce bright light with colors ranging from green to deep ultraviolet; however the efficiency of green and deep UV is low.

One of the key issues for increasing the efficiency of the devices is the reduction in dislocations, as they act as nonradiative recombination centers.[1] The generation of misfit dislocations (MDs) is a well-known phenomenon in heteroepitaxy, where a thin epilayer is grown on a substrate with significantly different lattice parameters. Below a certain epilayer thickness, called the *critical thickness* (CT), h_c, an epilayer may be grown pseudomorphically on a substrate, while a relaxation of misfit strain via plastic flow occurs for thicker epilayers $h > h_c$. The most common mechanism of plastic relaxation is through the formation of MDs.

Several models have been developed over the years for calculating the CT. Matthews and Blakeslee[2] proposed a model based on force equilibrium for the bending of preexisting threading dislocations. Fischer *et al.*[3] developed another force equilibrium model using an image-force method. People and Bean[4] and Freund and Suresh[5] described energy balance models for infinite MDs in cubic SiGe or GaAs systems. The models were later adopted for III-nitride systems despite the fact that the CT formulas were initially derived for isotropic materials, i.e., without considering the hexagonal symmetry of wurtzite nitrides. It was recently concluded that hexagonal symmetry results in lowering the CT by 10%–20% when compared with the isotropic values.[6] It was further shown that agreement of experimental data for the CT in the InGaN/GaN system was best using the energy balance model modified for hexagonal symmetry.[6]

In this paper, we employ some recent results of atomistic calculations[7–9] and show that the inclusion of the dislocation core energy term in CT considerations leads to significant changes in the results given by the energy balance model. Theoretical predictions will be compared with experimental data from the InGaN/GaN structures described below, as well as using a wide variety of data from the literature.

II. CRITICAL THICKNESS MODEL

The energy balance model compares the energy E_d of a MD added to the system with the work W done by the misfit stress field during the introduction of the dislocation (misfit energy relief). As a consequence, the CT criterion is given by

$$E_d + W = 0. \tag{1}$$

Assuming that the free surface and the epilayer-substrate interface are both (0001) planes, the formula for the work done by the misfit stress field (per unit length of the dislocation) is (see Appendix A for details)[6]

$$W = \frac{(c_{11}+c_{12})c_{33} - 2c_{13}^2}{c_{33}} \varepsilon_m b_{e,\parallel} h, \tag{2}$$

where h is the layer thickness, c_{ij} are the elastic constants, $b_{e,\parallel}$ is the edge component of the dislocation's Burgers vector lying in the epilayer-substrate interface, and ε_m is the misfit strain.

Regarding the dislocation energy (i.e., the energy introduced into the material), we note that the energy of a dislocation is comprised of two contributions

[a]Electronic mail: dh331@cam.ac.uk.

$$E_d = E_{\text{elastic}} + E_{\text{core}}. \tag{3}$$

E_{elastic} is the elastic energy outside the dislocation core, described by the cutoff radius r_c, and E_{core} is the energy of the dislocation core itself. The core energy is usually neglected (partly because it is often unknown) or is added to the elastic term in an empirical way.

A. Elastic part of the dislocation energy

The elastic contribution to the dislocation energy is usually expressed within the isotropic approximation. However, in our recent paper[6] we discussed the effect of hexagonal symmetry on the dislocation energy and concluded that it may significantly affect the CT. Within the hexagonal approximation, the elastic part of the dislocation energy is given by (see Appendix B for details)

$$E_{\text{elastic}}^{\text{hex}} = A_{\text{cont}} \ln\frac{R}{r_c} = (Ab_{e,\parallel}^2 + Bb_{e,\perp}^2 + Cb_s^2)\ln\frac{R}{r_c}, \tag{4}$$

where A, B, and C are numerical constants related to the elastic properties, $b_{e,\perp}$ is the edge component of the Burgers vector perpendicular to the epilayer-substrate interface, and b_s is the screw component of the Burgers vector. Our earlier calculations[6] were done with a core cutoff radius of $0.5b$ (where b is the length of the Burgers vector). This value was based on conclusions given in standard textbooks[10,11] and on the discussion of the CT by Freund and Suresh.[5]

B. Energy of the dislocation core

Recent atomistic results suggest that the core cutoff radius should be larger: Belabbas *et al.*[7] calculated a value $\approx b$ for the $(a+c)$-type dislocation in GaN, whereas Lymperakis[8] and Kioseoglou *et al.*[9] calculated $\approx 2b$ for the a-type dislocation in GaN. The CT calculation using these core radii instead of $0.5b$ (as used in our earlier work[6]), but without including the core energy term, for an InGaN single layer on a GaN substrate yields even lower values for the CT than those reported in Ref. 6 for the three different slip systems $\frac{1}{3}\langle 11\bar{2}0\rangle\{0001\}$, $\frac{1}{3}\langle 11\bar{2}3\rangle\{1\bar{1}01\}$, and $\frac{1}{3}\langle 11\bar{2}3\rangle\{11\bar{2}2\}$ considered there. Furthermore, the model without including the core energy term "breaks" [i.e., does not give any value for the CT as Eq. (1) does not have a solution] for indium content larger than $\approx 15\%$ (see the dashed lines in Fig. 1).

It is important to note that all the above mentioned atomistic calculations deal with dislocation lines along the $\langle 0001\rangle$ direction, whereas the MDs in our case lie in the (0001) plane, i.e., along either the $\langle 11\bar{2}0\rangle$ or the $\langle 1\bar{1}00\rangle$ direction (see Fig. 2). Up to now, there has been no report on similar atomistic calculations for dislocations along the latter two directions giving an estimation of the dislocation core energy and radius. Consequently, the atomistic results reported so far *do not* correspond to the MDs relevant to the CT calculations. Nevertheless, we will use these atomistic results as a first approximation.

The atomistic calculations provide not only an estimate of the core cutoff radii but also the core energy E_{core} for these dislocations in GaN.[7–9] Assuming that E_{core} does not change too much with the indium content, we can add it as a constant contribution to E_{elastic} in E_d into Eq. (1) and recalculate the CT curves. Such a correction has been mentioned before, for example, by Hu[12] for the SiGe system. However, it has been explored neither in detail nor for III-nitrides. The results are shown in Fig. 1 as the solid lines. Notice that the model now does not "break" at all in the case of hexagonal symmetry. Moreover, compared with the results without the core energy term, the CT values have increased, reflecting the increased dislocation energy. The model still remains quite simple but under the present approach retains more physics.

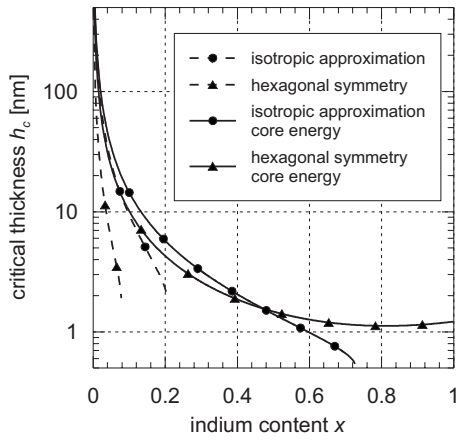

FIG. 1. CT curves for a single layer of InGaN on GaN for the $\frac{1}{3}\langle 11\bar{2}3\rangle \times\{1\bar{1}01\}$ slip system with the MD along $\langle 11\bar{2}0\rangle$ (see Fig. 2). The dashed and solid lines correspond to the results without and with the dislocation core term, respectively. The dislocation core radius and energy used are taken from Ref. 7.

The same physics can now be applied to another system of practical interest, an AlGaN epilayer grown on top of a GaN substrate. This system is under tensile strain, and thus strain relief is more often observed by cracking of the epilayer. Nevertheless, MDs have also been observed;[13] the results shown in Fig. 3 correspond to these situations.

Dislocation core parameters from the atomistic calculations (dislocation core energy E_{core}, core radius r_c, and the prelogarithmic term A) are summarized in Table I. We used the lowest energy configuration, which is the 5/7-atom ring for all Burgers vectors.[7–9] The prelogarithmic terms A_{cont}, as obtained from Eq. (4), are also included so that a comparison with values that result from the atomistic calculations can be made. Although the line directions of the MDs, which lie in

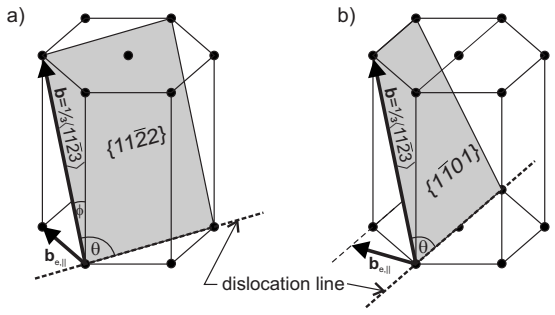

FIG. 2. The two prismatic slip systems considered here: (a) $\frac{1}{3}\langle 11\bar{2}3\rangle \times\{11\bar{2}2\}$ and (b) $\frac{1}{3}\langle 11\bar{2}3\rangle\{1\bar{1}01\}$. The component $b_{e,\parallel}$ of the Burgers vector from Eq. (2) is indicated and differs for the two systems, as shown.

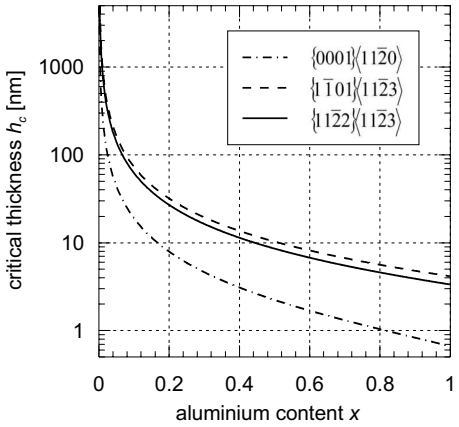

FIG. 3. CT curves for a single layer of AlGaN on GaN for three different slip systems. Calculations include the contribution of the dislocation core energy [taken from Refs. 7 and 9 for the $(a+c)$- and a-type dislocations, respectively].

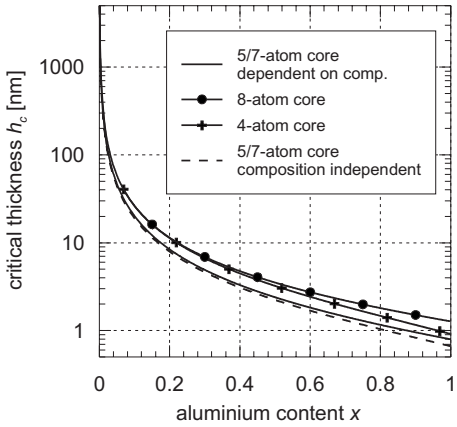

FIG. 4. CT curves for a single layer of AlGaN on GaN with the $\{0001\}\times\langle 11\bar{2}0\rangle$ slip system. The dashed and solid lines correspond to the energetically lowest dislocation core configuration with the 5/7-atom ring with and without taking into account the composition dependence of the core energy [after Ref. 9], respectively. The solid lines with crosses and disks correspond to the 4- and 8-atom ring dislocation core configurations, respectively.

the (0001) plane, do not correspond to those used in the atomistic calculations, the prelogarithmic terms correspond well, which makes us believe that the assumptions made here are reasonable.

C. Different dislocation core configurations

Kioseoglou *et al.*[9] provided a detailed study of the a-type dislocations along the $\langle 0001\rangle$ direction in III-nitrides. Consequently, using their results we are able to estimate the effect of neglecting the dependence of E_{core} on the composition x. The 5/7-atom ring core configuration is the configuration with the lowest energy for AlN, GaN, and InN.[9] Therefore, we take

$$E_{\text{core}}(\text{Al}_x\text{Ga}_{1-x}\text{N}) = xE_{\text{core}}(\text{AlN}) + (1-x)E_{\text{core}}(\text{GaN}) \quad (5)$$

and a similar expression for $\text{In}_x\text{Ga}_{1-x}\text{N}$. For comparison, we also considered other dislocation core configurations (4- and 8-atom rings) as discussed by Kioseoglou *et al.*[9] The results for AlGaN and the $\frac{1}{3}\langle 11\bar{2}0\rangle\{0001\}$ slip system are shown in Fig. 4. From this figure it is clear that the assumption of a composition independent core energy does not affect the results significantly (compare dashed and solid lines in Fig. 4). Different core configurations give the same CT in the case of the InGaN/GaN system and a slightly higher CT in the case of AlGaN/GaN compared with the CT for the 5/7-atom ring core, as shown in Fig. 4. One should also note that in the case of InGaN/GaN, the CT ranges down to 0.4 nm for $x=0.6$ (not shown here). Due to the fact that the dislocation core radius is about ≈ 0.7 nm (Table I), our CT estimations lose any physical sense below ≈ 1 nm.

TABLE I. Parameters of the 5/7-atom ring dislocation cores as resulting from the atomistic calculation [after Ref. 7 $(a+c)$-type and Ref. 9 a-type]. A_{cont} is the prelogarithmic term from Eq. (4).

Material	Dislocation	r_c (nm)	E_{core} (eV/Å)	A (eV/Å)	A_{cont} (eV/Å)
GaN	$(a+c)$-type	0.72	3.12	2.15	2.12
GaN	a-type	0.60	1.61	0.80	0.81
AlN	a-type	0.83	1.71	0.83	0.90
InN	a-type	0.54	1.66	0.56	0.41

III. EXPERIMENT

A number of InGaN epilayers with different thicknesses and compositions were deposited on thick GaN/sapphire pseudotemplates by metalorganic vapor-phase epitaxy in a Thomas Swan 6×2 in. close-coupled showerhead reactor. In addition, a series of five period InGaN/GaN multiple quantum well (MQW) structures was grown, in which the QW composition between the samples was changed. In a final MQW sample designed for transmission electron microscopy (TEM) analysis, the composition in each individual well was varied at a constant nominal thickness with the first well grown with the lowest indium fraction and the last one the highest. The five different QWs are separated by 100 nm thick GaN barriers. The barriers may be considered to be thick enough not to allow strain propagation from the underlying QW to the next QW. As a consequence, this sample is equivalent to five different layers grown on a GaN buffer.

For x-ray diffraction (XRD) analysis, a P'ANalytical MRD high resolution x-ray diffractometer (HR-XRD) was used to determine the indium content and layer thicknesses.

Cross-sectional TEM samples were prepared using a standard method: a sandwich structure was ground and polished down to 20–30 μm, followed by ion milling using a Gatan precision ion polishing system to obtain an electron transparent area. To observe dislocations in the samples, a Philips CM30 electron microscope was used in both bright field (BF) and dark field (DF) imaging modes.

A. Experimental results

The thickness and indium content of the InGaN epilayers A, B, and C were determined by comparing simulated curves with the experimental HR-XRD data.[14] The widths of the five QWs listed as D to H were determined by TEM using an edge-on imaging condition, as shown in Fig. 5. The indium content of the individual QWs was subsequently determined

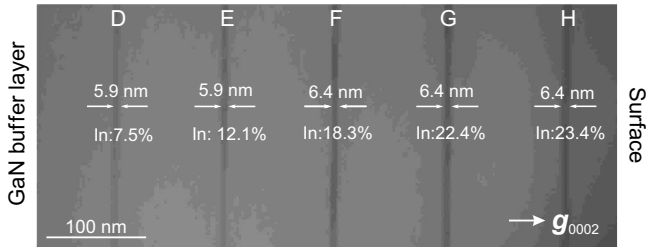

FIG. 5. BF image of the cross section of the MQW sample with QWs D to H taken at the edge-on condition.

by HR-XRD from the five QW structures grown with the individual QWs under the same conditions. The thicknesses and indium fractions of the InGaN epilayers and QWs are summarized in Table II.

Figure 6 shows the cross section of sample A that has the highest indium content and the largest thickness in the series of InGaN epilayers. Two reflections, $\mathbf{g}=0002$ and $\mathbf{g}=11\bar{2}0$, were used so that dislocations of all types could be observed. No MDs were observed in this InGaN epilayer. The threading dislocations that propagate from the underlying GaN buffer layer are observed to result in V-defects at the surface. In samples B and C, no MDs were observed either.

Figure 7 shows cross-sectional BF and DF images of the MQW sample. Additional threading dislocations are formed in the top two barriers, indicating that MDs are formed at the GaN/InGaN interface and bend ~90° to thread upward. The TEM measurements show that the top three QWs are slightly thicker than the bottom two, and from the test QW structures it was established that their indium fraction should increase in the order F, G, and H. Therefore, the CT may be reached for G and H QWs, and relaxation has occurred by the generated MDs. The additional threading dislocations could only be observed at the imaging condition $\mathbf{g}=11\bar{2}0$ (and not $\mathbf{g}=0002$), indicating their pure *a*-type character.

IV. DISCUSSION

In this section, we present a comparison of the CT curves shown above with the available experimental data (Figs. 8 and 9). Although the basal slip system $\frac{1}{3}\langle 11\bar{2}0\rangle \times\{0001\}$ is not operable for glide under the misfit strain in the wurtzite III-nitrides,[15] there are experimental observations of *a*-type MDs (see e.g., Refs. 16 and 17 and also this work). Such dislocations can neither glide from the free top surface nor be introduced by bending over a pre-existing threading dislocation using gliding. There are several hypotheses for their origin, for example, a "punch-out" mechanism [product of a reaction of two $(a+c)$-type dislocations glided from the top free surface][18] or a V-defect apex acting as a dislocation source.[19] However, more experimental work is needed to clarify this issue.

TABLE II. The thickness and indium fraction of the $In_xGa_{1-x}N$ epilayer and MQW samples measured with XRD and TEM.

	InGaN epilayers		
Sample	A	B	C
Thickness (nm)	39.7	33.5	36.6
Indium fraction *x*	13.3	2.8	8.4

	InGaN MQWs				
Sample	D	E	F	G	H
Thickness (nm)	5.9	5.9	6.4	6.4	6.4
Indium fraction *x*	7.5	12.1	18.3	22.4	23.4

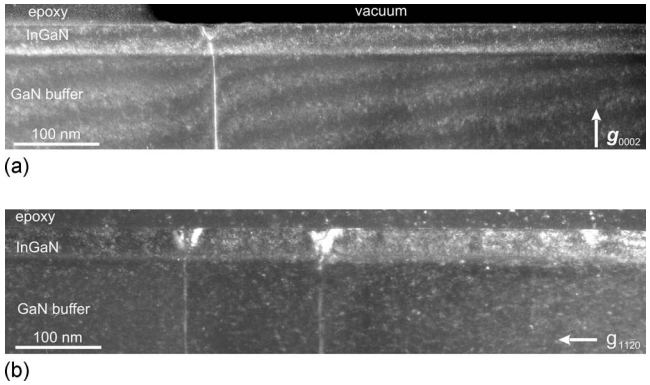

FIG. 6. DF image of the cross section of sample A using reflections (a) $\mathbf{g}=0002$ and (b) $\mathbf{g}=11\bar{2}0$. No MD was observed in the sample.

The present theoretical model predicts an equilibrium CT, which does not account for the actual MD generation mechanism. Therefore, theoretical CT values for both the basal $\frac{1}{3}\langle 11\bar{2}0\rangle\{0001\}$ and prismatic $\frac{1}{3}\langle 11\bar{2}3\rangle\{11\bar{2}2\}$ slip systems are shown in the following graphs 8 and 9 while noting that the experimental onset of *a*-type dislocations [unlike the $(a+c)$-type MDs] is expected to be significantly higher than the predicted CT values due to the inoperability of the basal slip system. However, if the punch-out mechanism for creation of the *a*-type dislocations by reaction of the $(a+c)$- and $(a-c)$-type dislocations proposed by Liu *et al.*[18] exists, then the CT values for the prismatic slip system would apply also to the *a*-type dislocations, which may be the reason for better agreement with experimental data.

Figure 8 shows results for AlGaN/GaN. The experimental data seem to follow quite closely the CT curve for the prismatic slip system. Note that including the dislocation core energy term in the model gives a CT curve which better resembles experimental data. Cracks are usually the first de-

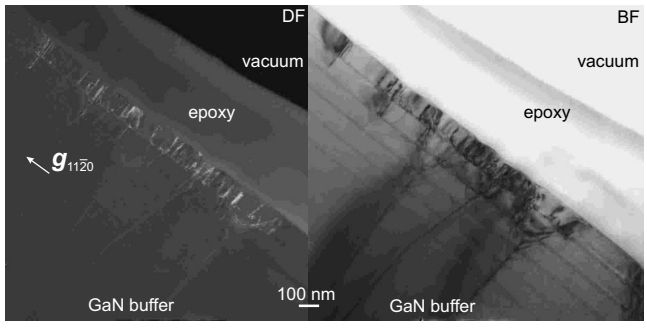

FIG. 7. DF (left) and BF (right) images of the cross section of the MQW sample using reflection $\mathbf{g}=11\bar{2}0$. Additional threading dislocations are seen to be generated in the top two InGaN QWs.

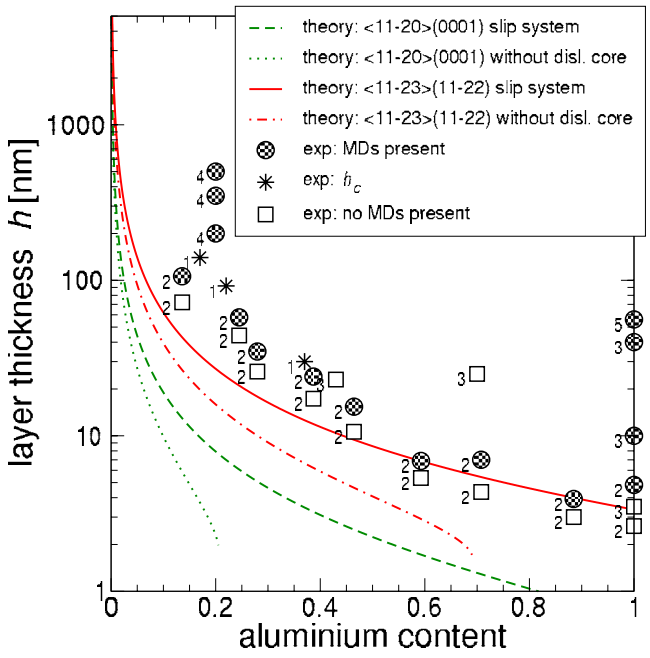

FIG. 8. (Color online) Comparison of theoretical predictions of the CT with experimental observations for the AlGaN/GaN system. Calculations were done for the basal $\frac{1}{3}\langle 11\bar{2}0\rangle(0001)$ and prismatic $\frac{1}{3}\langle 11\bar{2}3\rangle(11\bar{2}2)$ slip systems with the core radii $r_0=2b$ and $r_0=b$, respectively. Both CT curves with and without including the dislocation core energy term are shown. Experimental data were taken from following papers: (1) Floro *et al.* (Ref. 13), (2) Lee *et al.* (Ref. 20), (3) Vennéguès *et al.* (Ref. 21), (4) Bethoux and Vennéguès (Ref. 22), and (5) Gherasimova *et al.* (Ref. 23).

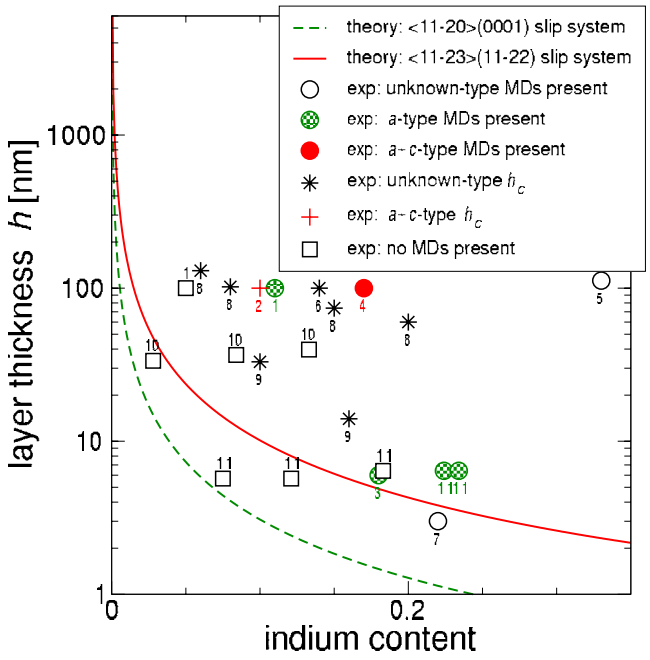

FIG. 9. (Color online) Comparison of theoretical predictions of the CT with experimental observations for the InGaN/GaN system. Calculations were done for the basal $\frac{1}{3}\langle 11\bar{2}0\rangle(0001)$ and prismatic $\frac{1}{3}\langle 11\bar{2}3\rangle(11\bar{2}2)$ slip systems with the core radii $r_0=2b$ and $r_0=b$, respectively. Experimental data were taken from following papers: (1) Liu *et al.* (Ref. 17), (2) Srinivasan *et al.* (Ref. 15), (3) Lü *et al.* (Ref. 16), (4) Liu *et al.* (Ref. 18), (5) Cho and Yang (Ref. 24), (6) Jahnen *et al.* (Ref. 19), (7) Costa *et al.* (Ref. 25), (8) Parker *et al.* (Ref. 26), (9) Reed *et al.* (Ref. 27), (10) epilayer samples A, B, C, and (11) QWs D, E, F, G, and H.

fect observed in AlGaN/GaN systems. This is expected to push the experimental onset of MDs to higher epilayer thicknesses when compared with the theoretical predictions in which MDs are the only strain relieving mechanism.

Figure 9 shows a similar comparison for the InGaN/GaN system. Here, information about the Burgers vector is available in many publications. The theoretical curves underestimate the CT with respect to the experimental data for both MD types, i.e., a-type and $(a+c)$-type Burgers vectors. V-defects, which also relieve misfit strain, are often observed experimentally and were also found in our observations (see Fig. 6). Together with the fact that the present model evaluates the equilibrium CT, these are probably the reasons for the discrepancy between the theory (in which the only strain relieving mechanism are MDs) and experiment.

In both graphs (Figs. 8 and 9), the data points labeled as "exp h_c," i.e., experimentally determined CT, are higher than the corresponding theoretical curves. There are two reasons for this. First, the present model predicts the equilibrium CT, i.e., when it first becomes energetically favorable to relieve misfit strain by introducing MDs. However, it does not take into consideration any mechanism for their actual generation, which may require an activation energy. Second, some frequently used experimental techniques (for example, photoluminescence and TEM) are unable to catch the very onset of misfit strain relief.[28]

It is worth noting that many of these observations were performed on samples grown on substrates with a low threading dislocation density. This rapidly reduces the possibility of creating MDs by bending pre-existing threading dislocations. Thus, if the generation of fresh MDs is prevented, the experimental CT is expected to increase due to the unavailability of low energy sources for MDs. We may also speculate that, in fact, V-defects and MDs are two competing strain relieving mechanisms. For low indium concentrations, V-defects are favored over MDs and the whole strain relaxation is governed by only V-defects. On the other hand, for higher indium concentrations when the misfit strain exceeds some critical value, V-defects alone are not sufficient anymore and thus MDs are introduced in order to help the relaxation process. This may then explain why we did not observe any MDs in our samples with low indium content (V-defects were always present).

V. CONCLUSIONS

We have reported experimental studies on MDs generated at the interfaces between InGaN/GaN heterostructures. We did not observe any MDs in the three InGaN epilayer samples with indium fractions ranging up to 0.133. In the sample with MQWs we observed MDs at the interfaces between the GaN barriers and the two InGaN QWs with the highest indium contents ($x>0.22$). The 100 nm thick barriers are assumed to be thick enough to prevent the stress fields of the QWs from mutual interactions.

We have shown the importance of atomistic calculations for equilibrium CT calculations that are usually treated only within continuum elasticity theory. It is worth noting that we have discussed here misfit strain relief *only* due to MDs;

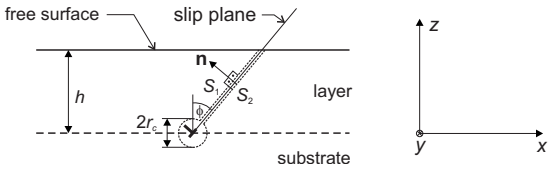

FIG. 10. The coordinate system and the cut plane for the cut-displace-weld procedure used for the estimation of the dislocation energy as described in the text. The Burgers vector **b** lies in the slip plane.

neither V-defects (InGaN/GaN systems) nor cracks (AlGaN/GaN systems) were addressed. A complex model taking into account all these defects is beyond the scope of this paper.

Recent atomistic results on the properties of dislocations in III-nitrides have been incorporated into the standard CT model, which show that in the case of thin epilayers and QWs, the energy contribution of the dislocation core is substantial. CT calculations taking into account the core energy agree better with experiment for both the AlGaN/GaN and InGaN/GaN systems than the standard theory ignoring the core energy.

ACKNOWLEDGMENTS

The authors acknowledge the EU project PARSEM (Contract No. MRTN-CT-2004-005583) and the EPSRC-GB (Contract No. EP/E035167/1) for financial support.

APPENDIX A: DERIVATION OF THE WORK *W*

Let us assume that the dislocation line is along the y-direction of the Cartesian coordinate frame and the wurtzite c-direction is parallel to the z-axis (see Fig. 10). The top surface of a specimen is stress free and therefore $\sigma_{zz}^m=0$. The only nonzero components of the uniform biaxial misfit stress are $\sigma_{xx}^m=\sigma_{yy}^m=\sigma_m$ within the thin layer. All directions within the xy-plane (the hexagonal c-plane) are equivalent, and thus the misfit strain components are $\varepsilon_{xx}^m=\varepsilon_{yy}^m=\varepsilon_m$. From Hooke's law it follows that,

$$0=\sigma_{zz}^m=c_{13}\varepsilon_{xx}^m+c_{13}\varepsilon_{yy}^m+c_{33}\varepsilon_{zz}^m \rightsquigarrow \varepsilon_{zz}^m=-2\frac{c_{13}}{c_{33}}\varepsilon_m. \quad \text{(A1)}$$

Using again Hooke's law, the misfit stress takes the form

$$\sigma_m=\sigma_{xx}^m=\frac{(c_{11}+c_{12})c_{33}-2c_{13}^2}{c_{33}}\varepsilon_m. \quad \text{(A2)}$$

Following Freund and Suresh,[5] the work W done by the mismatch stress while bringing the unit length of the dislocation from the free surface to its position in the interface is

$$W=\int_{h/\cos\phi}^{0}\sum_{i,j}b_i\sigma_{ij}n_j d\ell, \quad \text{(A3)}$$

where ℓ is the coordinate along the slip plane that is perpendicular to the dislocation line. The integrand is constant along the integration path. As a consequence, Eq. (A3) results in

$$W=-b\sigma_m h\sin\phi\sin\theta, \quad \text{(A4)}$$

where the following relations were used:

$$\mathbf{b}=\begin{pmatrix}-b\sin\phi\sin\theta\\ b\cos\theta\\ b\cos\phi\sin\theta\end{pmatrix},\quad \hat{\sigma}^m=\begin{pmatrix}\sigma_m & 0 & 0\\ 0 & \sigma_m & 0\\ 0 & 0 & 0\end{pmatrix},$$

$$\mathbf{n}=\begin{pmatrix}-\cos\phi\\ 0\\ \sin\phi\end{pmatrix}. \quad \text{(A5)}$$

It follows that $b_{e,\|}=-b\sin\phi\sin\theta$. Here, ϕ is the angle between the slip plane and a normal to the substrate-epilayer interface, and θ is the angle between the Burgers vector and the dislocation line.

APPENDIX B: DISLOCATION ENERGY FORMULA IN DETAIL

The derivation of Eq. (4) is a straightforward generalization of the procedure described by Willis *et al.*[29] for isotropic materials and by Steeds[30] for anisotropic materials. Here, only the final set of equations needed for the calculations presented here is given. The reader is referred to the above mentioned works[29,30] for more details.

A dislocation may be produced by making a cut along the intended slip plane, displacing one cut surface relative to the other by the Burgers vector **b**, and welding the material back together. This is shown schematically in Fig. 10. The work done by this procedure transforms to (and is equal to) the energy of the dislocation. The difference between the displacements on the surfaces S_1 and S_2 equals the Burgers vector **b**. The dislocation energy can be expressed as

$$E_{\text{elastic}}=\frac{1}{2}\int_{S_2}\sum_{i,j}b_i\sigma_{ij}^d n_j dS+\frac{1}{2}\int_{\text{around core}}\sum_{i,j}b_i\sigma_{ij}^d n_j dS, \quad \text{(B1)}$$

where n_j now denotes the outer normal to the surface S_2. The latter part of Eq. (B1) is neglected in the present calculations. The outer cutoff radius is R; the dislocation core radius is denoted as r_c. Then one obtains

$$E_{\text{elastic}}=\frac{1}{2}\sum_{n=1}^{3}[B_n(-b_x p_n+b_z)-C_n b_y+B_n^*(-b_x p_n^*+b_z)-C_n^* b_y]\ln\frac{R}{r_c}, \quad \text{(B2)}$$

where $B_3=0$, $C_1=0$, and $C_2=0$. Additionally, $p_3=i\sqrt{s_{44}/s_{66}}$, p_1, p_1^*, p_2, and p_2^* are solutions of the characteristic equation

$$\left(s_{33}-\frac{s_{13}^2}{s_{11}}\right)+\left(2s_{13}+s_{44}-2\frac{s_{12}s_{13}}{s_{11}}\right)p^2+\left(s_{11}-\frac{s_{12}^2}{s_{11}}\right)p^4=0 \quad \text{(B3)}$$

and $C_3=C_3^*=-b_y/(4\pi\sqrt{s_{44}s_{66}})$. B_1, B_1^*, B_2, and B_2^* are solutions of the following system of equations:

$$\sum_{n=1}^{2}(B_n p_n-B_n^* p_n^*)=0, \quad \text{(B4)}$$

$$\sum_{n=1}^{2}(B_n - B_n^*) = 0, \tag{B5}$$

$$b_x = 2\pi i\left(s_{11} - \frac{s_{12}^2}{s_{11}}\right)\sum_{n=1}^{2}(p_n^2 B_n - p_n^{*2} B_n^*), \tag{B6}$$

$$b_z = 2\pi i\left(s_{33} - \frac{s_{13}^2}{s_{11}}\right)\sum_{n=1}^{2}\left(\frac{B_n}{p_n} - \frac{B_n^*}{p_n^*}\right). \tag{B7}$$

s_{ij} are components of the compliance tensor (reflecting the correct hexagonal symmetry); b_i are components of the Burgers vector **b**.

The coefficients A, B, and C used in Eq. (4) are obtained from Eq. (B2) after solving the above described system of equations for a particular material system.

[1] S. J. Rosner, E. C. Carr, M. J. Ludowise, G. Girolami, and H. I. Erikson, Appl. Phys. Lett. **70**, 420 (1997).
[2] J. W. Matthews and A. E. Blakeslee, J. Cryst. Growth **27**, 118 (1974).
[3] A. Fischer, H. Kühne, and H. Richter, Phys. Rev. Lett. **73**, 2712 (1994).
[4] R. People and J. C. Bean, Appl. Phys. Lett. **47**, 322 (1985).
[5] L. B. Freund and S. Suresh, *Thin Film Materials: Stress, Defect Formation, and Surface Evolution* (Cambridge University Press, Cambridge, 2003).
[6] D. Holec, P. M. F. J. Costa, M. J. Kappers, and C. J. Humphreys, J. Cryst. Growth **303**, 314 (2007).
[7] I. Belabbas, A. Bere, J. Chen, S. Petit, M. A. Belkhir, P. Ruterana, and G. Nouet, Phys. Rev. B **75**, 115201 (2007).
[8] L. Lymperakis, Ph.D. thesis, Department Physik der Fakultät für Naturwissenschaften an der Universität Paderborn, 2005.
[9] J. Kioseoglou, P. Komninou, and T. Karakostas (unpublished).
[10] J. P. Hirth and J. Lothe, *Theory of Dislocations*, 2nd ed. (Krieger Publishing Company, Malabar, Florida, 1982).
[11] D. Hull and D. J. Bacon, 4th ed. *Introduction to Dislocations* (Butterworth-Heinemann, Oxford, 2002).
[12] S. M. Hu, J. Appl. Phys. **69**, 7901 (1991).
[13] J. A. Floro, D. M. Follstaedt, P. Provencio, S. J. Hearne, and S. R. Lee, J. Appl. Phys. **96**, 7087 (2004).
[14] M. E. Vickers, M. J. Kappers, T. M. Smeeton, E. J. Thrush, J. S. Barnard, and C. J. Humphreys, J. Appl. Phys. **94**, 1565 (2003).
[15] S. Srinivasan, L. Geng, R. Liu, F. A. Ponce, Y. Narukawa, and S. Tanaka, Appl. Phys. Lett. **83**, 5187 (2003).
[16] W. Lü, D. B. Li, C. R. Li, and Z. Zhang, J. Appl. Phys. **96**, 5267 (2004).
[17] R. Liu, J. Mei, S. Srinivasan, F. A. Ponce, H. Omiya, Y. Narukawa, and T. Mukai, Appl. Phys. Lett. **89**, 201911 (2006).
[18] R. Liu, J. Mei, S. Srinivasan, H. Omiya, F. A. Ponce, D. Cherns, Y. Narukawa, and T. Mukai, Jpn. J. Appl. Phys., Part 2 **45**, L549 (2006).
[19] B. Jahnen, M. Albrecht, W. Dorsch, S. Christiansen, H. P. Strunk, D. Hanser, and R. F. Davis, MRS Internet J. Nitride Semicond. Res. **3**, 39 (1998).
[20] S. R. Lee, D. D. Koleske, K. C. Cross, J. A. Floro, K. E. Waldrip, A. T. Wise, and S. Mahajan, Appl. Phys. Lett. **85**, 6164 (2004).
[21] P. Vennéguès, Z. Bougrioua, J. M. Bethoux, M. Azize, and O. Tottereau, J. Appl. Phys. **97**, 024912 (2005).
[22] J.-M. Bethoux and P. Vennéguès, J. Appl. Phys. **97**, 123504 (2005).
[23] M. Gherasimova, G. Cui, Z. Ren, J. Su, X.-L. Wang, J. Han, K. Higashimine, and N. Otsuka, J. Appl. Phys. **95**, 2921 (2004).
[24] H. K. Cho and G. M. Yang, J. Cryst. Growth **243**, 124 (2002).
[25] P. M. F. J. Costa, R. Datta, M. J. Kappers, M. E. Vickers, C. J. Humphreys, D. M. Graham, P. Dawson, M. J. Godfrey, E. J. Thrush, and J. T. Mullins, Phys. Status Solidi A **203**, 1729 (2006).
[26] C. A. Parker, J. C. Roberts, S. M. Bedair, M. J. Reed, S. X. Liu, and N. A. El-Masry, Appl. Phys. Lett. **75**, 2776 (1999).
[27] M. J. Reed, N. A. El-Masry, C. A. Parker, J. C. Roberts, and S. M. Bedair, Appl. Phys. Lett. **77**, 4121 (2000).
[28] D. J. Eaglesham, E. P. Kvam, D. M. Maher, C. J. Humphreys, G. S. Green, B. K. Tanner, and J. C. Bean, Appl. Phys. Lett. **53**, 2083 (1988).
[29] J. R. Willis, S. C. Jain, and R. Bullough, Philos. Mag. A **62**, 115 (1990).
[30] J. Steeds, *Introduction to Anisotropic ElasticityTtheory of Dislocations* (Clarendon, Oxford, 1973).